Analyst

ROYAL SOCIETY OF CHEMISTRY

PAPER

View Article Online
View Journal | View Issue

Cite this: *Analyst*, 2020, **145**, 2767

A handheld continuous-flow real-time fluorescence qPCR system with a PVC microreactor†

Bing Shi, [a,b] Yuanming Li, [a] Di Wu [a,b] and Wenming Wu *[a]

The polymerase chain reaction (PCR) has unique advantages of sensitivity, specificity and rapidity in pathogen detection, which makes it at the forefront of academia and application in molecular biology diagnosis. In this study, we proposed a hand-held real-time fluorescence qPCR system, which can be used for the quantitative analysis of nucleic acid molecules. For the first time, we use a PVC microreactor which improved the transmittance of the microreactor and made it easy to collect the fluorescence signal. In order to make it portable, the system adopted a passive syringe for sample injection and integrated temperature control and detection with a lithium battery for power supply. What's more, the fluorescence signal was captured by using a smartphone through an external automatic robotic arm. This real-time qPCR system can detect genomic DNA of the H7N9 avian influenza over four orders of magnitude of concentration from 10^7 to 10^4 copies per μL. In addition, it was verified that the fluorescence images obtained by this system were clearer than those obtained by a traditional system (using a PTFE spatial PCR microreactor) with two typical dyes and a probe tested—EvaGreen, SYBR Green and FAM.

Received 24th September 2019,
Accepted 2nd February 2020

DOI: 10.1039/c9an01894h

rsc.li/analyst

1. Introduction

Micro total analysis systems (μTAS) can be regarded as a miniaturization of the functions of an analytical laboratory integrated into a portable inch-scale microchip. During the last decade, μTAS have demonstrated significant functions in various fields, including the environment,[1] biology,[2,3] physics[4,5] and medicine.[6,7] One important application of μTAS is quantitative real-time PCR (qPCR), which has been widely used for detecting and quantifying the specific nucleic acid content in various fluids. μTAS have been widely applied in various fields, such as clinical disease diagnosis[8] and food safety,[9] showing their specificity, reliability and accuracy.

However, commercial qPCR instruments are bulky, expensive and complicated to operate. The portability of the qPCR thermocycler has been a target for researchers for a long time. For the traditional chip called the two-dimensional (2D) microchip, the reaction is carried out on a plane. In 1998,[10] Manz *et al.* developed a spatial PCR microreactor through three temperature zones using a serpentine channel. Since the first spatial PCR microreactor was reported, great progress has been made in PCR microfluidic technology. The common microchip materials are polydimethylsiloxane (PDMS),[11] polymethylmethacrylate (PMMA),[12,13] polytetrafluoroethylene (PTFE),[14] glass,[15] silicon,[16] polycarbonate (PC),[17] and fluorinated ethylene propylene (FEP).[18] However, the common material of a spatial PCR microreactor is polytetrafluoroethylene (PTFE), which has high temperature resistance and a low friction coefficient.[19] Although PTFE is more suitable for PCR microfluidic chips, the color of PTFE is milky white which makes it difficult for light to pass through it.

Not only that, until now, almost all spatial PCR systems have continued to rely on large off-chip devices, such as pump sources, computers, detection instruments and power supplies.[20,21] It remains a big challenge for researchers to realize a miniaturized continuous-flow PCR thermocycler model. In addition, all previous efforts in the miniaturization of continuous flow on-chip PCRs have been restricted to ordinary PCRs.[22] These restrictions have impeded their portability and application in more areas. In the last decade, with the vigorous development of microelectronics technology, some researchers have proposed a small-scale device based on smartphones[23,24] to solve this problem. In fact, smartphone cameras[25] have been used as fluorescence acquisition devices.[26–28] However, there are hidden dangers in the parallel synchronization of electronic devices which are controlled only by software, which often lead to missed shooting.

[a]*State Key Laboratory of Applied Optics, Changchun Institute of Optics, Fine Mechanics and Physics (CIOMP), Chinese Academy of Sciences, Changchun, 130033, China. E-mail: wuwm@ciomp.ac.cn*

[b]*University of Chinese Academy of Sciences (UCAS), Beijing, 100049, China*

†Electronic supplementary information (ESI) available. See DOI: 10.1039/c9an01894h

Here, we transformed a large commercial thermo-electric cooler/commercially available hot plate[29,30] into a portable heater band, and replaced the heavy mechanical pump with an external plug in a disposable syringe[31,32] as a passive micro-pump. A high transmittance material (polyvinyl chloride [PVC]) was used to make microreactors. A smartphone and a self-designed automatic cycle counting and photographing system were used for fluorescence acquisition. All devices were powered by portable lithium batteries. The three common DNA fragments of plasma isolated influenza virus (H7N9 avian influenza) plasmid, bacterium (*Escherichia coli*) plasmid, and hepatitis B virus (HBV) were tested. The average response efficiency of this system is 85% of that of a commercial PCR instrument (CFX Connect, Bio Rad). The average transmittance of the PVC microreactor is 1.67 times higher than that of the PTFE microreactor in qPCR amplification.

2. Experimental

2.1 Materials and methods

A PVC tube (0.3 mm ID) was purchased from Jieke Plastic Materials (China). Polydimethylsiloxane (PDMS) and a curing agent were purchased from Dow Corning. SYBR Premix Ex Taq II was purchased from Takara (Japan). EvaGreen was purchased from Biotium (USA). Plasmid and premade primers were purchased from Genweiz (China). A magnetic Serum/Plasma Circulating DNA Kit was obtained from TARGENE MEDICAL (China).

2.2 Composition of the handheld continuous-flow fluorescence analytical system

The assembled handheld continuous-flow real-time qPCR system (Fig. 1) measures 16 × 14 × 10 cm^3. It is powered by three 18 650 lithium batteries with a total capacity of 3500 mA h and an operating voltage of 12 V. The average power of the system during operation is 9 W. After the system is fully charged, it can work continuously for about 4.66 hours in a single operation. This system consists of three sections: the temperature control subsystem, sample propulsion subsystem and fluorescence acquisition subsystem.

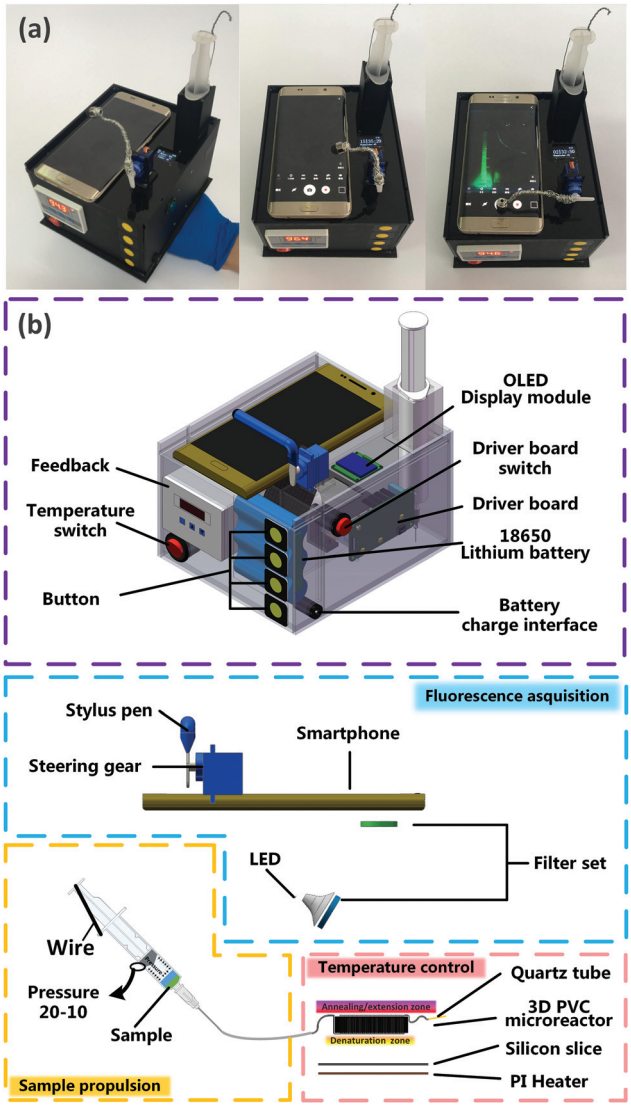

Fig. 1 (a) The photos of the handheld continuous-flow real-time fluorescence qPCR system. (b) The schematic diagram of the real-time qPCR system which has three sections: temperature control, sample propulsion and fluorescence acquisition.

2.3 PVC microreactor and temperature control

The temperature control device consists of a PVC microreactor, a polyimide (PI) heater, a silicon slice and a temperature-controlled feedback device. The PVC microreactor includes a PVC tube and PDMS block, in which the PDMS block acts as a physical support for the whole microreactor. The PVC tube (ID = 0.3 mm, OD = 0.7 mm) is rotated around an isosceles trapezoid PDMS block (two parallel sides are 0.7 cm and 3 cm, a height of 0.9 cm and a length of 4 cm). The tube is wound around the PDMS block, and the PDMS block is wrapped and fixed with a black tape. The 45 rotations of the PVC tube on the PDMS block correspond to the 45 thermal cycles, each of which requires a 7 cm-long tube with a total length of 350 cm. A 3 cm-long quartz tube (ID = 0.1 mm, OD = 0.36 mm) is connected using cyanoacrylate glue (502 glue) at the outlet of the PVC tube to make a blunt-ended fluidic conduit and produce a stable flow velocity in the microreactor. The PI heater is placed at the bottom of the microreactor so that two temperature zones can be realized on the upper and lower surfaces of the PVC microreactor (the thermal image of the PVC microreactor is shown in Fig. S1†). The temperature gradient is formed because the temperature gradient changes along the vertical direction, in which the lower layer represents the denaturation temperature, while the upper layer of the microreactor indicates the annealing temperature of the target, as shown in Fig. 1b. The annealing temperature of the target for amplification can be freely adjusted by changing the height of the microreactor, and the temperature can be accurate up to ±0.2 °C. Due to the 3D configuration of the microreactor, the

temperature regime generated at the top of the isosceles trapezoid structure was different from that at the bottom, which made the microreactor become a flexible and common system for the flow of various PCR samples. Because the portable PI heater is only 1 mm thick and can achieve a fast response to temperature rise and fall, its polyimide hot film has excellent insulation, resistance, thermal conductivity and resistance stability, and high temperature control accuracy. The variation of denaturation temperature can be controlled accurately up to ±2 °C by feedback. However, due to the non-uniform heating caused by the design of the heater, a silicon slice was placed between the PVC microreactor and the PI heater to achieve uniform heating of the denatured zone.

2.4 Sample propulsion

Prior to using the microreactor for PCR, the samples needed to be pushed. The traditional injection method requires large mechanical pumps to push the samples, the greatest advantage of which is the constant speed. However, its disadvantages include a large volume and the need for an external power supply, which make the miniaturization and portability of the PCR equipment more difficult. In the present study, the self-activated flow injection method was adopted. The operation method of the experimental equipment and procedures for constructing the hand-held pumping device using a disposable plastic syringe are as follows. First, the microreactor tube was filled with mineral oil. The syringe was injected with a little mineral oil (about 2 mL). The outlet part of the PVC tube is connected with a 3 cm long quartz tube, which is made blunt-ended by clamping. Second, a small amount of mineral oil was injected into the front end of the needle (needle [27G]) using a glass syringe. Then, 30 μL of the PCR mixture with fluorescence dyes was added into the mineral oil. The piston was pulled to the brim of the syringe connected to the inlet of the PVC tube, clamped with a clip at the microreactor outlet part, and then pushed to the predetermined graduation of the syringe (the piston pushed from 20 to 10), causing the pressure to increase. Finally, the piston is fixed at the position mentioned above with a wire, as shown in Fig. 1b.

2.5 Fluorescence acquisition and analysis

2.5.1 Subsystem composition. The smartphone fluorescence acquisition subsystem consists of a smartphone (South Korea), a light emitting diode (LED) (China), two narrowband filters (China), a stylus pen and a steering gear. The excitation light from the LED with a dominant wavelength of 475 nm and a power of 3 W was used to excite the fluorescence dyes in the PCR mixture, which is filtered by a center wavelength of 480 nm (bandwidth 8 ± 2 nm), irradiating the upper surface of the microreactor with a downward angle of 30°. A narrowband filter with a center wavelength of 520 nm (bandwidth 8 ± 2 nm) was used to filter the fluorescence during the PCR, while the real-time fluorescence image was observed using the smartphone. The camera of the smartphone was placed 6.5 cm above the upper surface of the microreactor. Compared to some previous literature studies,[33] the dichroic mirror was removed from this system, which made the structure simple and eliminated the signal interference of excitation light. The automatic photography function is realized by the control of the stylus by the steering gear (the operation principle is described in detail in section 2.5.2). Real-time fluorescence imaging can be completed by merely using the imaging function of the mobile phone, which reduces some system debugging processes, and the captured images are clearly visible (see "Results and discussion" Fig. 3a). The image capture settings were set as a focal length of 2.8 mm, F = 0.5, and ISO 400 in real-time quantitative PCR. The captured fluorescence images can be transmitted to servers in wireless or wired mode, so that these images can be processed rapidly and the amplification curves can be generated. As for real-time fluorescence image analysis by using the ImageJ software, the green channel information was restored by segmenting the RGB channels of the fluorescence image. The average intensity of the rectangle (30 pixels × 300 pixels) of each image was extracted. The relationship between the fluorescence intensity and period was plotted.

2.5.2 Operation principle of automatic photography. In order to realize a fully programmable automation process, the present study designed a special automatic cycle counting and photographing system, which mainly included the central microprocessor module, the power LED driver module, the rudder driver module, the OLED display module, the key input module, the buzzer module and the power management module with a specific system block diagram, as shown in Fig. 2a. The photo interval, lighting time and photo-duration can be set by the key input module and OLED display module, respectively, according to the specific system block diagram presented in Fig. 2b. After the system starts, it automatically enters the parameter setting interface. The operator can set the number of photos, the interval and the lighting time using the "SET", "UP", "DOWN" and "BACK" keys on the system. Based on the above setting, the system can automatically calculate the total test time as the reference for testers, which can be adjusted from 40 minutes and 12 seconds to one hour, 15 minutes and 32 seconds. When all the parameters are set correctly, press the "SET" button for a long time to enter the working state. The countdown function of the photo interval can be realized by precise timing of the internal timer of the central microprocessor. When the countdown reaches zero, the system enters the imaging state and drives a strong blue LED to illuminate the microreactor. After the PCR mixture with fluorescence dyes enters the microreactor, the controlling gear (steering gear) rotates the fixed angle, and the image is taken by clicking the mobile phone. After the image is taken, it reenters the countdown state of the image interval. This operation continues until the number of images reaches the presetting, quits the working state, and completes the single image test. In addition, the system can set up the lighting intensity of the strong blue light LED in order to achieve an ideal photo effect. At the same time, the rotation angle of the steering machine can be set freely to adapt to different imaging equipment and mechanical structures of the shell.

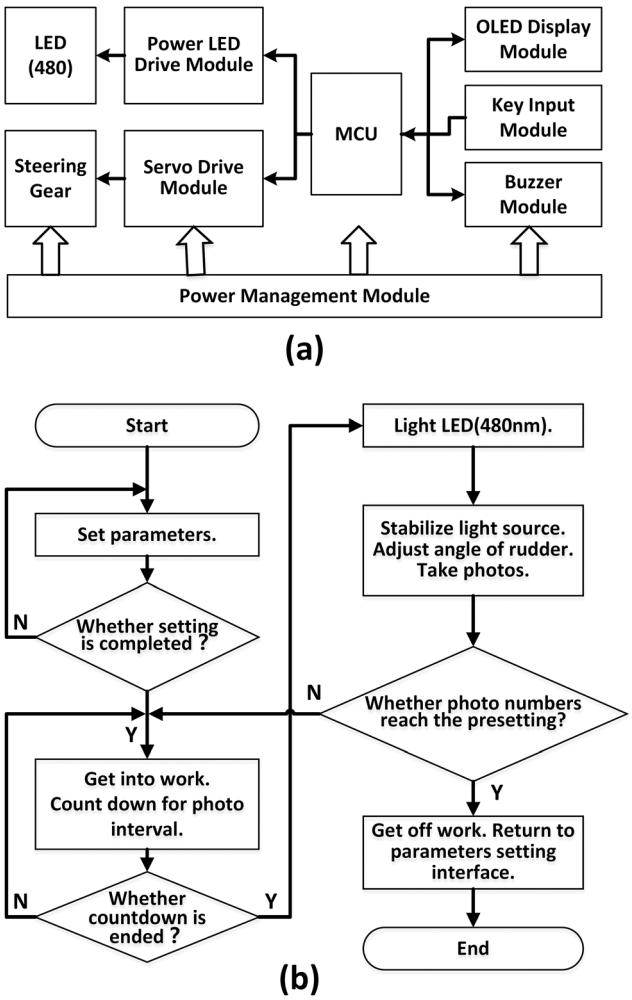

Fig. 2 (a) Structure composition of the stylus pen photographing section; (b) work-flow diagram of the stylus pen photographing section.

The system can use the smartphone, the compact system camera and the SLR camera. This system has advantages of simple portability, low power consumption, convenient operation, wide application, and so on. It has a program upgrade interface that facilitates the upgrade and maintenance of subsequent software.

3. Results and discussion

3.1 Real-time quantitative detection in the handheld continuous-flow fluorescence analytic system

By detecting the plasmids embedded in H7N9 avian influenza DNA with continuous-flow real-time PCR assays, the capacity for high-speed quantification of the handheld continuous-flow fluorescence analytical system was demonstrated. Fig. 3a presents the fluorescence images under the amplifiers with concentrations ranging from 10^7 to 10^4 copies per μL. Fig. 3b shows that amplification curves were generated by extracting the fluorescence intensity peak of five different concentrations of PCR

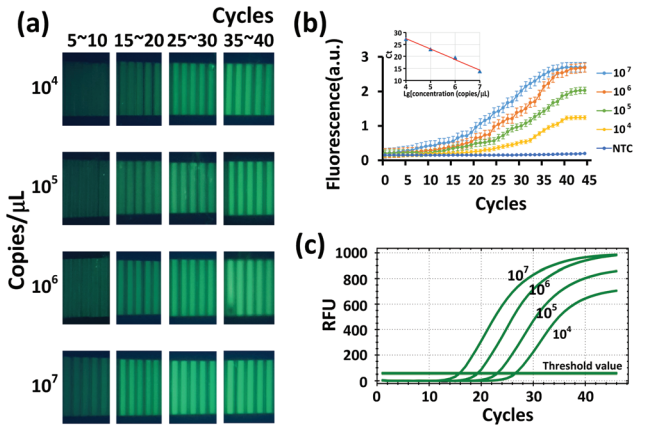

Fig. 3 The handheld continuous-flow fluorescence analytical system for real-time quantitative detection of DNA molecules of H7N9 avian influenza. (a) Typical fluorescence images of continuous-flow PCR amplicons amplified from 10^7 to 10^4 copies per μL of DNA molecules. (b) Amplification curves of the fluorescence images from the handheld continuous-flow fluorescence analytical system. Ct values for DNA concentrations spanning over 4 orders of magnitude. Error bars are the standard deviations. (c) Amplification curves of the fluorescence images from the commercial PCR instrument (CFX Connect, Bio Rad).

reagents in each cycling channel after three repeated experiments. The Ct values[34] of the four curves were calculated to be 14.84, 19.52, 22.96 and 27.27, with the R^2 value calculated to be 0.9901 for the microreactor. It can be intuitively seen from the fluorescence curve at different concentrations of the DNA template respectively generated amplification reactions in different cycle channels. Fig. 3c shows the amplification curves of the fluorescence images from the commercial PCR instrument (CFX Connect, Bio Rad). For instance, for 10^7 copies per μL DNA, the amplification reactions can be seen to begin at approximately the 15th cycle. In addition, for 10^4 copies per μL DNA, the amplification reactions can be seen to begin at approximately the 30th cycle. Therefore, the handheld continuous-flow fluorescence analytical system can rapidly carry out accurate quantitative detection.

3.2 Transmittance comparison and fluorescence assays

The transmittance properties of the PVC and PTFE tubes have a great influence on the stimulated excitation light and emission light passing through the microchannel wall, thereby affecting the detection sensitivity of the fluorescence signal during microfluidic processing, such as qPCR. In order to estimate the difference in the light transmittance of PVC and PTFE, the transmittance of PVC and PTFE thin films of 0.5 mm, 1 mm, and 1.5 mm, respectively, was analyzed by using a spectrophotometer, as shown in Table 2. The transmittance of three PVC films and PTFE films with different thicknesses is shown in Fig. 4a. From the comparison of these three sets of data, it is easy to see that the transmittance of the PVC film is much higher than that of the PTFE film not only for the excitation light (480 nm), but also for the emission light (520 nm). Based on the above data analysis, it can be con-

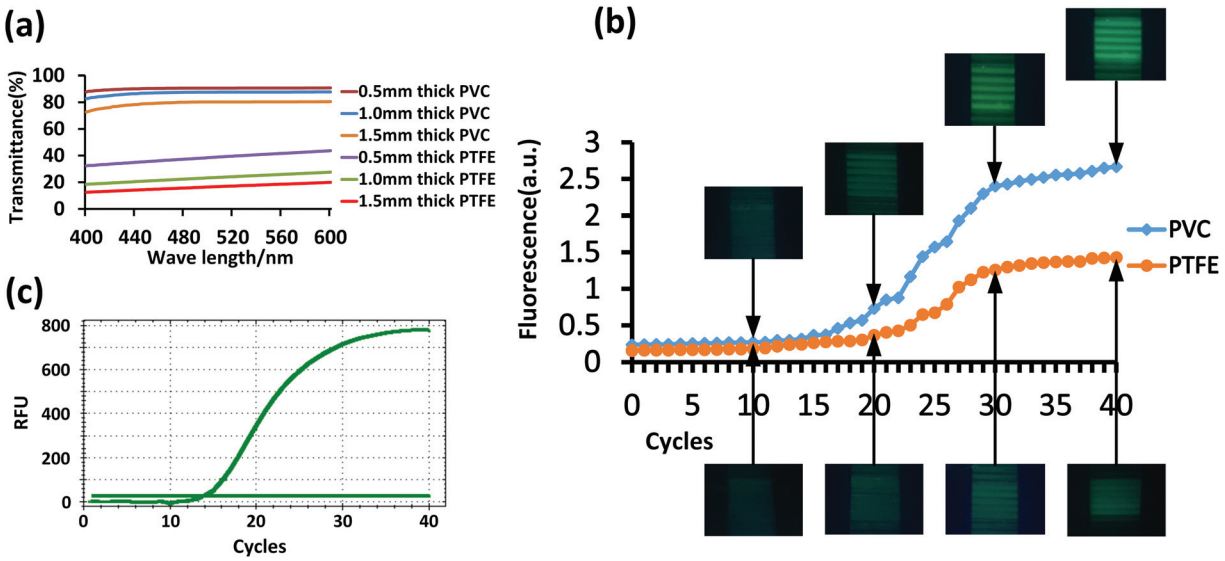

Fig. 4 Comparison of transmissivity for PVC and PTFE. (a) Under the conditions of the same illumination intensities and different wavelengths, the transmissivities of 5 mm, 10 mm, and 15 mm thick PVC and PTFE were compared. (b) The fluorescence curves of the same concentration of pGEM-3Zf (+) DNA molecules amplified in PVC and PTFE, and real-time fluorescence images in the 10th, 20th, 30th, and 40th cycle, respectively. (c) The fluorescence curves of pGEM-3Zf (+) DNA molecules amplified in the commercial PCR instrument (CFX Connect, Bio Rad).

cluded that the PVC material is superior to PTFE for fluorescence excitation and detection during qPCR.

In order to further demonstrate that the PVC film is better for fluorescence detection than the PTFE film, a PTFE microreactor of the same size as the PVC was made to simultaneously perform control experiments of continuous-flow real-time PCR assays for the DNA detection of pGEM-3Zf (+). PCR mixtures with EvaGreen passed into the PVC and PTFE microreactors, respectively, which were placed on the same heater to conduct the PCR under the same light conditions. The real-time fluorescence images obtained from three repetitive experiments were processed by software and the amplification curves are shown in Fig. 4b. Two curves represent the fluorescence amplification curves of pGEM-3Zf (+) DNA molecules with the same concentration in PVC and PTFE. The eight small pictures in Fig. 4b represent the real-time fluorescence images obtained at the 10th, 20th, 30th and 40th cycles, respectively. Fig. 4c shows the fluorescence curves of pGEM-3Zf (+) DNA molecules amplified in the commercial PCR instrument (CFX Connect, Bio Rad). As observed from the fluorescence curves, the fluorescence intensity collected from the PVC microreactor was significantly higher than that collected from the PTFE microreactor, which was approximately 1.67 times that of the PTFE microreactor. Because two narrow band filters were used in this PCR system for fluorescence detection, the narrowband filters filter out stray light, which is equivalent to the loss of some light energy, so that the natural light intensity will be weakened. And the properties of the PTFE material will enhance the fluorescence effect. So, the multiple relations of fluorescence transmittance captured by the smartphone were lower than the multiple relations of the spectrophotometer in Table 1. From the above results, it can be concluded that the PVC film has better transmittance, and it is more suitable for quantitative real-time PCR under the same external conditions.

3.3 Fluorescence contrast

In order to further prove that the PVC microreactor was better than the PTFE microreactor in real-time fluorescence detec-

Table 1 Primer sequence for influenza virus (H7N9 avian influenza) and bacterium (*Escherichia coli*)

Target	Sequence 5′···3′	Amplicon (bp)
H7N9 avian influenza	Fw TAC AGA CAA TCC CCG ACC GA Rv CCT ACC CCG ATT GTG AAC CG	116 bp
Escherichia coli pGEM-3Zf (+)	Fw CCA GTC GGG AAA CCT GTC GTG CC Rv GTG AGC GAG GAA GCG GAA GAG CG	99 bp

Table 2 Transmittance comparison of PVC and PTFE using a spectrophotometer

Material	PVC/PTFE	PVC/PTFE	PVC/PTFE
Thickness (mm)	0.5	1	1.5
Wavelength (nm)	600 → 400	600 → 400	600 → 400
Transmittance (%)	90.78 → 72.71/43.63 → 32.35	87.82 → 82.77/27.55 → 18.43	80.51 → 72.71/19.89 → 12.45

tion, three sets of 60 μL of PCR mixtures were taken, in which the concentration of template DNA was 10^6 copies per μL in each set. Among these, two sets were H7N9 avian influenza with fluorescence dyes of 1× EvaGreen and 1× SYBR Green, respectively, while the other set was HBV with the FAM fluorescent probe. These three sets of PCR mixtures were evenly divided into two parts, and fed into the PVC and PTFE microreactors, respectively, for real-time fluorescence photography, as shown in Fig. 5a–c.

Fig. 5a and b present the fluorescence images of the H7N9 avian influenza amplified at the 10th, 20th, 30th, and 40th cycle, using EvaGreen and SYBR Green, respectively. Fig. 5c shows the fluorescence images of HBV amplified at the 10th, 20th, 30th, and 40th cycle. The bar plots represent the fluorescence intensity of the DNA template amplified products in the PVC and PTFE microreactors, respectively. The comparison of amplification curves for the three PCR mixtures after the processing with the ImageJ software is shown in Fig. 5d. Fig. 5e and f present the electropherograms (the method of gel electrophoresis provides section II of the ESI†) of the amplification products of H7N9 and HBV, respectively. Horizontal axes correspond to the three sets of PCR reactions in Fig. 5a, b and c, while the vertical axes represent the average fluorescence intensity of electropherograms obtained by three repeated tests for each group of reagents processed by ImageJ software. As observed from the electropherograms and bar charts, the PCR reaction efficiency of the PVC and PTFE microreactors was almost the same. However, in each set of real-time fluorescence images and amplification curves, it can be clearly seen that the fluorescence intensity observed in the PVC microreactor is higher than that of the PTFE microreactor, regardless of which dye. Furthermore, the real-time fluorescence intensity observed in the PTFE microreactor is only 59% of that of the PVC microreactor. In conclusion, the PVC microreactor is better than the PTFE microreactor in the real-time qPCR field.

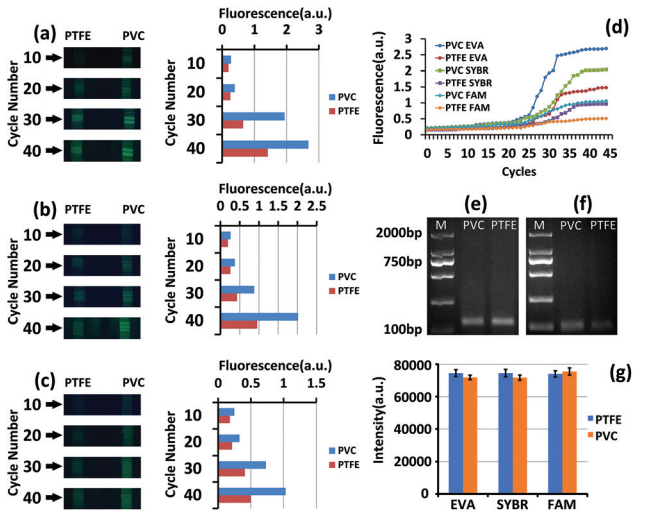

Fig. 5 The real-time quantitative fluorescence curves of the same concentration of DNA molecules amplified in PVC and PTFE using three different dyes. (a and b) The fluorescence images of H7N9 avian influenza with a concentration of 106 copies per μL amplified at the 10th, 20th, 30th, and 40th cycle using EvaGreen and SYBR Green dyes, respectively. (c) The fluorescence images of the hepatitis B virus (HBV) with the FAM probe at a concentration of 106 copies per μL, amplified at the 10th, 20th, 30th, and 40th cycle. (d) The amplification curves generated by the fluorescence images in (a)–(c). (e and f) H7N9 avian influenza and HBV amplified by the handheld continuous-flow fluorescence analytic system, respectively, in which lane M shows the DNA bands of the marker. (g) The intensity of the amplified H7N9 avian influenza and HBV of the handheld continuous-flow fluorescence analytic system. Three groups represent figures (a), (b) and (c), respectively, which show the average value of three times of amplifications of each group.

4. Conclusions

In summary, a handheld continuous-flow real-time qPCR system powered by lithium batteries for rapid, sensitive and quantitative molecular diagnosis was introduced. By integrating a PVC spatial PCR microreactor with smartphone fluorescence imaging for the first time, the handheld continuous-flow fluorescence analytical system can capture sharper fluorescence images. Moreover, when compared with a traditional PTFE spatial PCR microreactor using a PCR mixture, regardless of which dye, the fluorescence images obtained from the PVC spatial PCR microreactor are clearer. In general, the handheld continuous-flow fluorescence analytical system can achieve 104 or more copies per μL DNA of detection, and is able to achieve accurate DNA quantification with a dynamic range of four orders of magnitude. The handheld continuous-flow fluorescence analytical system has great application prospects in obtaining high brightness real-time fluorescence images, and it is portable and easy to operate. This work found that the transmittance of the PVC microreactor was very high, which was very helpful for the detection of qPCR. However, the PVC material is very soft. In the winding process when passing the corner of the PDMS block, the deformation of the PVC pipe due to tension results in the wall hanging phenomenon of the liquid section. So, we will focus on the design of the chip in future studies, so that the droplets can pass with uniform speed in the future for the digital PCR.

Conflicts of interest

There are no conflicts to declare.

Acknowledgements

This project was supported by the CAS Pioneer Hundred Talents Program, the National Natural Science Foundation of China (no. 61704169), the Natural Science Foundation of Jilin Province (20180520112JH), and the Talent Project of Jilin Province.

Notes and references

1 J. J. Wetz, A. D. Blackwood, J. S. Fries, Z. F. Williams and R. T. Noble, *Estuaries Coasts*, 2014, **37**, 421–435.
2 F. Habouzit, G. Gevaudan, J. Hamelin, J. P. Steyer and N. Bernet, *Bioresour. Technol.*, 2011, **102**, 4054–4060.
3 S. Petsch, S. Schuhladen, L. Dreesen and H. Zappe, *Light: Sci. Appl.*, 2016, **5**, e16068.
4 B. L. Fernandez-Carballo, I. McGuiness, C. McBeth, M. Kalashnikov, S. Borros, A. Sharon and A. F. Sauer-Budge, *Biomed. Microdevices*, 2016, **18**, 34.
5 W. Zhang, H. Zappe and A. Seifert, *Light: Sci. Appl.*, 2014, **3**, e145.
6 H. Deng, Q. Liu, X. Wang, R. Huang, H. Liu, Q. Lin, X. Zhou and D. Xing, *Biosens. Bioelectron.*, 2017, **87**, 931–940.
7 X. Yang, X. Zhou, M. Zhu and D. Xing, *Biosens. Bioelectron.*, 2017, **91**, 238–245.
8 B. L. Fernandez-Carballo, C. McBeth, I. McGuiness, M. Kalashnikov, C. Baum, S. Borros, A. Sharon and A. F. Sauer-Budge, *Anal. Bioanal. Chem.*, 2018, **410**, 33–43.
9 M. Zhen and H. Zhuang, *Food Anal. Methods*, 2018, **11**, 862–872.
10 M. U. Kopp, A. J. D. Mello and A. Manz, *Science*, 1998, **280**, 1046.
11 G. C. Santini, C. Potrich, L. Lunelli, L. Vanzetti, S. L. Marasso, M. Cocuzza, F. C. Pirri and C. Pederzolli, *Biophys. Chem.*, 2017, **229**, 142–150.
12 G. S. Lim, J. S. Chang, Z. Lei, R. Wu, Z. Wang, K. Cui and S. Wong, *Lab Chip*, 2015, **15**, 4032–4043.
13 J. H. Son, B. Cho, S. Hong, S. H. Lee, O. Hoxha, A. J. Haack and L. P. Lee, *Light: Sci. Appl.*, 2015, **4**, e280.
14 Y. Li, Y. Jiang, K. Wang and W. Wu, *Anal. Chem.*, 2018, **90**, 11925–11932.
15 N. Xue and W. Yan, *IEEE Sens. J.*, 2012, **12**, 1914–1918.
16 S. Petralia, R. Verardo, E. Klaric, S. Cavallaro, E. Alessi and C. Schneider, *Sens. Actuators, B*, 2013, **187**, 99–105.
17 W. Fan, B. K. Lok and F. K. Lai, *Proceedings of the 2016 IEEE 18th Electronics Packaging Technology Conference, EPTC 2016*, 2017, pp. 360–364.
18 A. C. Hatch, T. Ray, K. Lintecum and C. Youngbull, *Lab Chip*, 2014, **14**, 562–568.
19 H. Teng, *Appl. Sci.*, 2012, **2**, 496–512.
20 J. Chen, Z. Luo, L. Li, J. He, L. Li, J. Zhu, P. Wu and L. He, *Lab Chip*, 2018, **18**, 412–421.
21 B. L. Fernández-Carballo, I. Mcguiness, C. Mcbeth, M. Kalashnikov, S. Borrós, A. Sharon and A. F. Sauer-Budge, *Biomed. Microdevices*, 2016, **18**, 1–10.
22 B. Shi, G. He and W. Wu, *Mikrochim. Acta*, 2018, **185**, 467.
23 I. Hussain, K. U. Ahamad and P. Nath, *Anal. Chem.*, 2017, **89**, 767–775.
24 I. Hussain, K. U. Ahamad and P. Nath, *RSC Adv.*, 2016, **6**, 22374–22382.
25 Y. M. Park, Y. D. Han, H. J. Chun and H. C. Yoon, *Biosens. Bioelectron.*, 2017, **93**, 205–211.
26 V. Potluri, P. S. Kathiresan, H. Kandula, P. Thirumalaraju, M. K. Kanakasabapathy, S. Kota Sai Pavan, D. Yarravarapu, A. Soundararajan, K. Baskar, R. Gupta, N. Gudipati, J. C. Petrozza and H. Shafiee, *Lab Chip*, 2018, **19**, 59–67.
27 U. Obahiagbon, J. T. Smith, M. Zhu, B. A. Katchman, H. Arafa, K. S. Anderson and J. M. Blain Christen, *Biosens. Bioelectron.*, 2018, **117**, 153–160.
28 A. Priye, S. Wong, Y. Bi, M. Carpio, J. Chang, M. Coen, D. Cope, J. Harris, J. Johnson, A. Keller, R. Lim, S. Lu, A. Millard, A. Pangelinan, N. Patel, L. Smith, K. Chan and V. M. Ugaz, *Anal. Chem.*, 2016, **88**, 4651–4660.
29 K. T. L. Trinh, W. Wu and N. Y. Lee, *Microchim. Acta*, 2014, **181**, 1697–1705.
30 Y. Jiang, L. Du, Y. Li, Q. Mu, Z. Cui, J. Zhou and W. Wu, *Analyst*, 2018, **143**, 3798–3807.
31 W. Wu, K. T. Trinh and N. Y. Lee, *Analyst*, 2012, **137**, 983–990.
32 W. Wu, K. T. L. Trinh, Y. Zhang and N. Y. Lee, *RSC Adv.*, 2015, **5**, 12071–12077.
33 S. V. Angus, S. Cho, D. K. Harshman, J. Y. Song and J. Y. Yoon, *Biosens. Bioelectron.*, 2015, **74**, 360–368.
34 T. D. Schmittgen and K. J. Livak, *Nat. Protoc.*, 2008, **3**, 1101–1108.